

Evolution of Massive Stars

Up to the End of Central Oxygen Burning

M. F. El Eid¹

*Department of Physics,
American University of Beirut (AUB), Beirut, Lebanon*

meid@aub.edu.lb

and

B. S. Meyer and L.-S. The

*Department of Physics and Astronomy, , Kinard Laboratory of Physics,
Clemson University, Clemson, SC 29634-09789*

mbradle@clemson.edu

tlihsin@clemson.edu

ABSTRACT

We present a detailed study of the evolution of massive stars of masses 15, 20, 25 and 30 M_{\odot} assuming solar-like initial chemical composition. The stellar sequences were evolved through the advanced burning phases up to the end of core oxygen burning. We present a careful analysis of the physical characteristics of the stellar models. In particular, we investigate the effect of the still unsettled reaction $^{12}\text{C}(\alpha, \gamma)^{16}\text{O}$ on the advanced evolution by using recent compilations of this rate. We find that this rate has a significant impact on the evolution not only during the core helium burning phase, but also during the late burning phases, especially the shell carbon-burning. We have also considered the effect of different treatment of convective instability based on the Ledoux criterion in regions of varying molecular weight gradient during the hydrogen and helium burning phases. We compare our results with other investigations whenever available. Finally, our present study constitutes the basis of analyzing the nucleosynthesis processes in massive stars. In particular we will present a detail analysis of the *s*-process in a forthcoming paper.

¹Department of Physics and Astronomy, Kinard Laboratory of Physics, Clemson University, Clemson, SC 29634-0978

Subject headings: nuclear reactions, nucleosynthesis, abundances–stars: evolution–stars: interiors

1. INTRODUCTION

Study of the evolution of massive stars through the advanced burning phases up to the collapse of the iron core is an active and complex field of research in stellar astrophysics. However, this does not mean that the early hydrogen and helium burning phases are less important. Modeling stars is an initial value problem, and as we shall see in this paper, these early phases determine in a crucial way the initial conditions for the following burning phases, and the resulting stellar nucleosynthesis. Therefore, despite several recent works dealing with the late evolution of massive stars (e.g. Chieffi et al. 1998; Limongi et al. 2000; Woosley et al. 2002; Imbriani et al. 2001) an up-to-date, systematic study that also emphasizes the effect of the early stellar phases on the later ones seems useful as well as a discussion of uncertainties in key assumptions in the models.

The main emphasis of this paper, then, is an exploration of the physical conditions during the later burning phases of massive stars, how they are set by earlier burning stages, and how they are affected by uncertainties that remain in the input to the models. A proper understanding of these issues is important not only for clarifying the evolution of massive stars but also for an accurate accounting of the stellar nucleosynthesis.

In this work, we present a systematic discussion of the evolution of massive stars through the H, He, C, Ne, and O burning phases. We have made some effort to study the influence of uncertain physical assumptions on the evolution. In §2, we give a brief description of the stellar evolution code we have used in the present calculations. Section 3 and its subsections contain a detailed discussion of the characteristics of the burning phases mentioned above. In §4, we compare our results with those of other works. Section 5 contains our conclusions.

2. STELLAR EVOLUTION CODE

The stellar evolution code used in this work is generally described in The et al. (2000). As in our previous work, the nuclear reaction network in the code contains 632 nuclear species, which allows us to follow most stellar nucleosynthesis processes, including the *s*-process nucleosynthesis, in detail. For the present version of the code, we have updated the nuclear data. We now use nuclear masses from compilation of Audi & Wapstra (1995) and thermonuclear reaction rates from the compilation of the “NACRE” European collaboration

(Angulo et al. 1999), and the “Non-Smoker” compilation of Rauscher & Thielemann (2000).

In various stellar sequences described in §3, we have used different reaction rates for the reaction $^{12}\text{C}(\alpha, \gamma)^{16}\text{O}$, which is still unsettled. The latest compilation is due to Kunz et al. (2002). As stated in that work, the cross section of this reaction is extremely small (10^{-17} barn) at the energies relevant to core helium burning; therefore, one has to rely on measurements at higher energies to obtain the S-factor at the relevant stellar energies by extrapolation.

Kunz et al. (2002) seem to have succeeded in reducing the uncertainties in the evaluation of the cross section at stellar temperatures. Fig. 1 shows clearly a different temperature dependence of the rate obtained by Kunz et al. (2002) compared to other compilations. Normalized to the rate of Caughlan & Fowler (1988) (hereafter CF88), we see that we are dealing with a different rate in the range of helium burning ($1.3\text{--}3.7 \times 10^8$ K) and of carbon burning in the vicinity of $T_9 = 1$. The implication of this new rate will be discussed in §3 and 4.

3. CHARACTERISTICS OF THE BURNING PHASES

We present evolutionary sequences for stars of masses 15, 20, 25, and 30 M_\odot having solar-like initial chemical composition (Anders & Grevesse 1989). All the evolutionary sequences have been evolved up to the end of central oxygen burning. Most models included mass loss by stellar wind according to the semiempirical relation by de Jager et al. (1988) and used the Schwarzschild criterion for convection throughout the star. In order to study the effects of mass loss, the treatment of convective mixing in chemically inhomogeneous layers, and the uncertainty in the $^{12}\text{C}(\alpha, \gamma)^{16}\text{O}$ reaction rate, we calculated several evolutionary sequences with different input physics as summarized in Table 1. The only sequence calculated without mass loss is for the 25 M_\odot star (referred to as 25NM) in Table 1. The case 25N is the same as 25NM, but mass loss is included here. The case 25L is identical to 25N except that the Ledoux criterion for convection was adopted in the region of the H-burning shell (see §3.1 for details). In the sequence 25K, the rate for the reaction $^{12}\text{C}(\alpha, \gamma)^{16}\text{O}$ was used according to Kunz et al. (2002), instead of the NACRE rate used in 25N.

Fig. 2a shows the HR diagram for our four evolutionary sequences 15, 20, 25N, and 30 M_\odot . Physical characteristics of these tracks are described in §3.1 with help of Figs. 2b and 3.

Figs. 4–10 show the change of the internal structure of the stellar models at a given time for all sequences listed in Table 1. In these figures we have labeled all convective zones

according to their physical origin, whether due to nuclear burning in a core or in shell region, or in a star’s envelope, or in an intermediate convection zone (referred to as ICZ) formed in the outer stellar layers above the receding convective core during core H-burning. We will use these figures to describe the global characteristics of successive burning phases as they occur in our evolutionary models. Note that the ICZ in Figs. 4-10 contain the semiconvective and convective regions that move in time due to the gradient in hydrogen mass fraction and opacities. In our calculations we do not include semiconvective mixing but apply the Ledoux criterion in order to avoid introducing another parameter in our calculations which is so far needed for describing semiconvective mixing.

3.1. Hydrogen and Helium Burning Phases

It is well known that significant changes of the evolutionary tracks occur during the hydrogen and helium burning phases of massive stars; therefore, we show in Fig. 2a the evolutionary tracks in the HR-diagram for the stars under consideration. In all models, we adopt the Schwarzschild criterion for convection to determine the convective regions in a stellar model at a given time, except case 25L described below. The evolutionary tracks in Fig. 2a evolve nearly at constant luminosity after the main sequence phase until they finally reach the red giant branch (RGB). However, this evolution at constant luminosity and, more importantly, the timing to reach the RGB depend crucially on mass loss and on how convective mixing is treated in the stellar layers of variable molecular weight gradient (or simply μ -gradient) left behind the shrinking hydrogen convective core during the main sequence evolution.

To understand these issues, we may compare different evolutionary sequences as shown in Figs. 2b and 3. Fig. 2b shows the evolutionary tracks when mass loss is neglected as in our case 25NM, or when the convection treatment is different as in case 25L. These cases are discussed below. Fig. 3 shows the effective temperature T_{eff} as a function of the central helium mass fraction $X(^4\text{He})$ and demonstrates clearly how the evolution of the star to the RGB is influenced by mass loss. In the case of no mass loss, the star remains in the blue region of the HR diagram during most of its core He-burning. If mass loss is included, then the more massive the star, the stronger is the mass loss and the earlier is the transition to the RGB. In other words, this transition occurs at higher central helium mass fraction $X(^4\text{He})$ (see Fig. 3)

To explain the behavior of the evolutionary tracks further, we compare in detail the evolution of the $25 M_\odot$ star with and without mass loss. As Fig. 2b shows, the sequence 25NM (without mass loss) has higher luminosity during core hydrogen burning. This is

simply a consequence of the higher mass in this case. During core helium burning, however, the explanation is more complicated since now two energy sources are available in the star that contribute to the luminosity: a central source and shell source. Why is the luminosity of the sequence with mass loss lower?. We answer this question with the help of Figs. 6 and 9 showing the change of internal structure in the course of evolution for the sequences 25N and 25NM, respectively. In the early evolution through the hydrogen and helium burning phases, these figures show a remarkably different behavior of the convective zones that forms above the hydrogen-burning shell. In the sequence 25NM, this convective zone is more extended in mass and lasts throughout the whole core helium burning phase. In contrast, in sequence 25N, calculated with mass loss, the convective zone is narrower in mass and disappears before helium exhaustion in the core (at $X(^4\text{He}) \simeq 0.1$). The implication of this is that the H-burning shell in case 25NM is stronger because it is supplied by more fuel.

The stronger H-burning shell has several consequences on the ensuing evolution:

1. It leads to a higher luminosity of the star during core helium burning (see the tracks for the $25 M_\odot$ star in Fig. 2b).
2. It delays the evolution to the RGB. The star remains as a blue supergiant during most of its core helium burning phase (case 25NM in Fig. 3).
3. It prolongs the duration of the core helium burning owing to the slightly lower central temperature in the case without mass loss (see Table 3).
4. It leads to a larger mass of the hydrogen exhausted core (or simply helium core) $M_\alpha = 7.62 M_\odot$ in case 25NM compared to $M_\alpha = 7.51 M_\odot$ in case 25N (see Table 3).

We point out that all these features have been recognized by several authors (see Chiosi & Maeder (1986), for a review). We refresh this issue, because it is relevant to our present discussion.

A more pronounced change of the structure of the convective zone formed above the H-burning shell is found when the effect of the mean molecular weight (or simply μ -gradient) is taken into account to determine the extent of this convective zone. It is well known (for a basic discussion see Kippenhahn & Weigert 1990, §6) that the μ -gradient acts to inhibit convection. In this case, convection is no longer a dynamical instability, rather one deals with semiconvection, which is a consequence of thermal instability. The criterion for convection that should be applied in this case is the “Ledoux criterion”:

$$\nabla_{rad} > \nabla_{ad} + \frac{\varphi}{\delta} \nabla_\mu \quad (1)$$

where the ∇ 's are logarithmic gradients and the quantities φ and δ are derivatives obtained from the equation of state (see Kippenhahn & Weigert 1990). The second term ∇_μ is always positive and consequently inhibits convection. We will describe in the following the results we have obtained for an evolutionary sequence of the $25 M_\odot$ star (labeled 25L in Table 1), where we have applied the Ledoux criterion only in the region of varying μ -gradient, in which the H-burning shell is effective. Elsewhere in the stellar model, we have used the Schwarzschild criterion for convection. We emphasize that our treatment maximizes the choking effect of the μ -gradient on convection.

As mentioned above, layers of varying μ -gradient are semiconvective. There is no general theory that describes the efficiency of this process. When semiconvection is treated as a diffusion process (e.g., Langer et al. 1983, 1985; El Eid 1995; Woosley et al. 2002 for a recent discussion), then a parameterization of the diffusion coefficient for semiconvection is used. For our present investigation, we avoided using this kind of parameterization by including the whole effect of the μ -gradient. We adopt the Ledoux criterion in regions of varying μ -gradient in case 25L and otherwise use the Schwarzschild criterion. A similar approach has been done by Stothers & Chin (1992).

In the following, we summarize the different features in the evolution of the sequence 25L as compared to the case 25K during core helium burning. The choking effect of the μ -gradient on convection inhibits the formation of a convection zone above the H-burning shell (compare Figs. 8 and 6). There are two key consequences of this. First the H-shell source is weaker in 25L than in 25K, which explains the immediate evolution to the RGB as seen in Fig. 2b. Secondly, owing to the weaker H-burning shell, the mass of the convective core during core helium burning becomes larger in order to supply the luminosity of the star. In 25K, the maximum convective helium core mass is $5.32 M_\odot$ while in the case of 25L it is $6.16 M_\odot$. Therefore the H-shell is located farther out in mass in 25L. The helium core mass is $M_\alpha = 7.54 M_\odot$ for 25K, but $8.33 M_\odot$ for 25L.

In addition to the above effects, there are two other consequences of the weaker H-shell. First, the larger mass of the convective core leads to a shorter duration of core helium burning due to the higher central temperature: 6.88×10^5 yrs for 25L compared to 7.49×10^5 yrs for 25K. Second, in the case of a weaker H-shell, the He-shell burning occurs in a region $M_r = 6.184 - 8.108 M_\odot$, while in case 25K this region comprises $M_r = 5.393 - 7.290 M_\odot$. In other words, when the Ledoux criterion is used in the H-shell region, the He-burning shell migrates farther out by about $0.8 M_\odot$ compared to the case with Schwarzschild criterion everywhere in the stellar model.

It is interesting to note that our sequence 25L has many similarities with the sequence of the $25 M_\odot$ star calculated by Woosley et al. (2002) (hereafter WHW). We obtain close

agreement with these authors concerning the depth of the outer convective envelope and the He-burning shell. We achieve good agreement concerning the higher total mass lost from this star, because in both calculations the stellar sequences evolve directly to the RGB, after the main sequence phase, where mass loss increases significantly. Finally, we also find agreement for the mass of the helium core (see Table 6 for more details).

Summing up this discussion, then, the treatment of convective mixing in the region of varying μ -gradient where the H-burning shell is active affects many physical quantities relevant to the evolution past core helium burning.

In connection with the early evolution phases, we may also comment on the effects of mass loss and envelope convection on the surface abundances, which are modified when the stellar sequences reach the RGB and develop convective envelopes, such that the processed material is mixed to the surface (the well-known "first dredge up"). Table 2 shows the surface abundances as they result after the first dredge up for the stars under consideration. The ratio of $^{12}\text{C}/^{13}\text{C}$ decreases with increasing stellar mass (15, 20, 25N, and 30) owing to the larger production of ^{13}C by the CNO cycle in more massive stars. When mass loss is neglected as in case 25NM, this ratio becomes larger.

The ratio $^{14}\text{N}/^{15}\text{N}$ increases strongly with the stellar mass mainly due to the destruction of ^{15}N by the (p,α) reaction in the CNO cycle. At constant mass, ^{15}N is strongly reduced because convective mixing extends over a larger mass of the envelope. Eventually, the ratio $^{14}\text{N}/^{15}\text{N}$ may be used as indicator of mass loss.

The ratio $^{16}\text{O}/^{18}\text{O}$ is an increasing function of the stellar mass. Its behavior is similar to $^{14}\text{N}/^{15}\text{N}$, although its variation is not so strong.

In contrast to the behavior discussed above, the ratio $^{16}\text{O}/^{17}\text{O}$ does not have a monotonic dependence on the stellar mass. This is because the production and destruction of ^{17}O is rather sensitive to temperature variations influencing the reaction $^{17}\text{O}(\text{p},\alpha)^{14}\text{N}$ in particular. The effect of mass loss leads to a slight decrease of this ratio. The enrichment of sodium compared to solar ([Na/Fe] in Table 2) is an increasing function of the stellar mass owing to the more efficient Ne-Mg cycle in more massive stars.

It may be also interesting to compare the surface isotopic ratios of the the sequence 25L with those of 25N. As shown in Table 2, a significant difference is found for the ratios $^{14}\text{N}/^{15}\text{N}$, $^{16}\text{O}/^{18}\text{O}$ and [Na/Fe]. The isotopic ratios of the sequence 25N represent the products of shell hydrogen-burning which was operating at higher temperatures (by a factor of about two at the bottom of the shell) than in case 25L. This is clearly seen by the higher enrichment of Na, and the high destruction of ^{15}N and ^{18}O . These products are mixed to the surface from deeper stellar layers in case of 25N, where the convective envelope penetrates down to 7.6

M_{\odot} compared to $8.7 M_{\odot}$ in case 25L. We observe that the surface isotopic ratio in massive stars may depend on how convection is treated in the layer where shell hydrogen burning proceeds.

Table 3 presents a few more details about the stellar sequences listed in Table 1. As may be seen, the final masses of the helium cores, M_{α} of the stars under consideration are $3.85 M_{\odot}$ for the $15 M_{\odot}$, $5.70 M_{\odot}$ for the $20 M_{\odot}$, $7.53 M_{\odot}$ for the $25 M_{\odot}$ with mass loss, and $9.54 M_{\odot}$ for the $30 M_{\odot}$. As Table 3, indicates, M_{α} ceases to change at the end of core carbon burning. Our values above are in close agreement with the results by Nomoto & Hashimoto (1988) and Arnett (1996). However, we think that our results are more accurate because those authors followed the evolution of helium cores only, that is without including the H-burning shell in their calculations. We make another comparison with other authors in Table 6 (see §4).

We conclude this section by discussing a very important physical quantity determined at the end of core He-burning, namely, the central mass fraction of carbon, $X(^{12}\text{C})$. Table 4 shows that using the Kunz et al. (2002) reaction rate for $^{12}\text{C}(\alpha, \gamma)^{16}\text{O}$ leaves a larger $X(^{12}\text{C})$ than using the NACRE rate. As Fig. 1 shows, the Kunz et al. (2002) rate is lower than the NACRE rate for $T_9 < 0.4$, which explains why the former rate allows for less destruction of ^{12}C during the late stages of core helium burning. Interestingly, among the $25 M_{\odot}$ models, the lowest value of $X(^{12}\text{C}) - 0.193$ is obtained for the 25NM. This is due to the higher central temperature encountered in this case which leads to more efficient destruction of ^{12}C . The central $X(^{12}\text{C})$ strongly affects the subsequent evolution of the star (Woosley et al. 1993; Imbriani et al. 2001).

3.2. Carbon Burning Phase

In this section, we present some details about core and shell carbon burning. The evolution of the centers of the stars of masses 15 to $30 M_{\odot}$ in a $T_C - \rho_C$ diagram is shown in Fig. 11 where the ignition temperatures of the calculated burning phases are indicated by the dashed lines (see entry 5 in Table 3). Core carbon burning occurs in the temperature range $(0.32 - 1.2) \times 10^9 \text{ K}$ where the lowest value belongs to the $15 M_{\odot}$ star while the highest value belongs to the $30 M_{\odot}$ star.

Core carbon burning in the $15 M_{\odot}$ star occurs in a convective core whose mass reaches a maximum value of $0.55 M_{\odot}$. The duration of core carbon burning is 6760 yrs. When the carbon is exhausted in the core, shell-carbon burning mediates the evolution toward neon burning; in contrast to the helium-burning shell that has its location in mass radius fixed at

all times (see Figs. 4 - 10), carbon burning in a shell exhibits complicated behavior. In the $15 M_{\odot}$ model, two episodes of convective shell C-burning occurs before Ne-ignition where the shell advances in mass (see Fig. 4).

Core carbon burning in the $20 M_{\odot}$ star occurs in a convective core whose mass reaches a maximum of $0.49 M_{\odot}$. The duration of this phase is 3300 yrs. The shell C-burning proceeds here also in two convective episodes. We note that during the second episode, a broader convective zone is formed than in the $15 M_{\odot}$ model (see Fig. 5).

In the $25 M_{\odot}$ model (case 25N), core carbon burning occurs in a convective core whose mass reaches a maximum of $0.35 M_{\odot}$. In this case, there are three subsequent carbon shells. The last of these has a range of $(2.26 - 4.54) M_{\odot}$ and persists to the end of the calculation. How the shell C-burning proceeds depend crucially on the carbon profile created in the star after core C-burning. Fig. 12a and 12b show clear difference in such profile.

It is interesting to compare the effect of different rates for the reaction $^{12}\text{C}(\alpha, \gamma)^{16}\text{O}$ on carbon burning in the $25 M_{\odot}$ models. Comparison of Figs. 6 and 7 shows the structural evolution of the stellar sequences 25N and 25K as obtained from the Schwarzschild criterion for convection and the different rates of $^{12}\text{C}(\alpha, \gamma)^{16}\text{O}$ as in Table 1. As we saw previously in Table 4, $X(^{12}\text{C})=0.236$ is left at the end of core helium burning when the rate of $^{12}\text{C}(\alpha, \gamma)^{16}\text{O}$ according to NACRE is used, but $X(^{12}\text{C}) = 0.280$ according to Kunz et al. (2002). The larger $X(^{12}\text{C})$ at the end of core helium burning allows 25K to develop a convective core with a maximum mass of $0.47 M_{\odot}$ in contrast to $0.36 M_{\odot}$ for 25N.

It seems that the higher the value of ^{12}C , the larger is the mass of the convective core during core C-burning. This is due to the well-known interplay between the energy generation rate and neutrino loss rate (Arnett 1972; Woosley & Weaver 1986; Chieffi et al. 1998; Limongi et al. 2000). A convective core forms only when the effective energy generation rate (nuclear minus neutrino) is positive. The difference in the mass of the convective core has a consequence on the duration of core C-burning: it lasts 3500 yrs in case 25K, but 1600 yrs in case 25N.

It is also interesting to compare 25N to our sequence without mass loss designated as 25NM in Table 1 and Fig. 9. At the end of core He-burning, $X(^{12}\text{C}) = 0.193$. The low value of $X(^{12}\text{C})$ leads to a maximum mass of 0.23 for the convective core during core C-burning in 25NM, but a duration for this phase of 1860 yrs, longer than in 25N. While the mass of the convective core during core C-burning is correlated to $X(^{12}\text{C})$ at the beginning of this burning phase, the lifetime of this phase has no simple relation to $X(^{12}\text{C})$, because it depends also sensitively on how the center of the stars evolve in a $T_C-\rho_C$ plane. Fig. 13a shows this kind of evolution is rather complicated, which affects the nuclear energy generation rates

and the neutrino loss rates leading to the variation of the lifetime found above.

From Fig. 10 and Table 3, we see that the $30 M_{\odot}$ model has a maximum carbon-convective core mass of $0.39 M_{\odot}$. This mass is somewhat larger than that in 25N, even though the mass fraction of ^{12}C is larger in 25N than the $30 M_{\odot}$ model, an exception to the general rule that more carbon gives a larger convective carbon core. On the other hand, we note that at the time of core carbon burning, the $30 M_{\odot}$ star has in fact a lower mass than that of 25N. This and the complicated interplay between energy generation and neutrino energy loss obscure a direct relation between the convective core mass and $X(^{12}\text{C})$.

We now focus in more detail on shell C-burning, and consider in particular the $25 M_{\odot}$ sequences. As seen in Figs. 6 and 7, the shell C-burning starts in a first phase near the edge of the former convective core with a convective zone formed above the shell. A second convective phase of this shell burning comprises more mass in the sequence 25K than in 25N. How C-shell burning proceeds depends crucially on the carbon profile left in the star after core C-burning.

Fig. 12a and 12b help to illustrate this point. They show the composition profile of major elements at the end of core Ne burning. The profile of carbon at this stage is clearly different. In the sequence 25K, the second convective phase of C-shell burning comprises more mass compared to that of the sequence 25N. Consequently, C-shell burning in 25K is stronger and leads to a significantly reduced carbon abundance in the mass range $1.5 - 4.0 M_{\odot}$ (see Fig. 12a as compared to Fig. 12b. Clearly, the rate of $^{12}\text{C}(\alpha, \gamma)^{16}\text{O}$ has a significant effect on the properties of the shell C-burning.

To complete the discussion, we point out that a convective core of $0.55 M_{\odot}$ is formed (see Fig. 12b) in the $15 M_{\odot}$ sequence during core C-burning and that shell C-burning proceeds in two convective episodes prior to Ne ignition. By contrast, in the $30 M_{\odot}$ sequence, the mass of the convective core is $0.39 M_{\odot}$ (see Fig. 10) and C-shell burning constitutes only one single convective episode.

When the core C-burning ends and the stars contract toward core Ne-ignition, a third convective C-shell episode starts in all our cases except in the $30 M_{\odot}$ sequence. This third convective C-shell lasts all the time as far as we have carried out calculations beyond core O-burning. Indeed this last phase of C-shell burning seems to survive till core collapse as it is seen in the calculations carried to the collapse phase (Chieffi et al. 1998; Limongi et al. 2000; Woosley et al. 2002).

3.3. Neon Burning Phase

For the stars under consideration, core Ne-burning occurs in the temperature range $(1.2 - 1.9) \times 10^9$ K (see entry 7 in Table 3). A characteristic of this burning phase is that a convective core is always formed in the mass range of $0.6 - 0.75 M_\odot$, but it exists only during a short time interval during which the effective energy generation rate (nuclear - neutrino) is positive; thus, core Ne-burning is partially radiative and of short duration (3.13 yrs for the $15 M_\odot$, 1.21 yrs for the $20 M_\odot$, 0.33 yrs for the $30 M_\odot$).

The effect of the rate for the reaction $^{12}\text{C}(\alpha, \gamma)^{16}\text{O}$ is also encountered during this phase. Comparing the sequences 25K and 25N, we find that the convective core attains a maximum mass of $0.61 M_\odot$ for 25N, but $0.75 M_\odot$ for 25K. The lifetime of core Ne-burning is rather different: 0.294 yrs for 25N, but 3.28 yrs for 25K.

The shorter lifetime of the sequence 25N is not only a consequence of the relatively smaller mass of its convective core, but it can also be traced back to the effect of $^{12}\text{C}(\alpha, \gamma)^{16}\text{O}$. Sequence 25K achieves a larger central mass fraction of Ne at the end of core carbon burning (0.384, see Table 4). As Figs. 13a and 13b show, this larger Ne mass fraction allows the sequence 25K to evolve at relatively lower central temperatures but higher densities during core Ne-burning than the sequence 25N. It also results in a pronounced expansion phase during core Ne burning, as seen in Fig. 13a. The longer lifetime of core Ne-burning in 25K than in 25N is thus due to fact that 25K has more Ne to burn and does so at relatively lower temperatures.

In the $25 M_\odot$ models, the third convective phase of C-shell burning occurs during core Ne-burning. A significant difference exists in this phase between 25K and 25N. In 25K, the convective zone above the C-shell is quite narrow in mass. This is due to the fact that the mass fraction of ^{12}C is relatively high throughout the helium exhausted core; therefore, when carbon burning occurs during the second convective phase of the C-shell, the burning is vigorous, which gives an extended second carbon convective shell and largely depletes the ^{12}C . This makes less carbon available for the third convective carbon shell, which, consequently weaker and narrower. It is interesting to see that the effect of the rate for $^{12}\text{C}(\alpha, \gamma)^{16}\text{O}$ propagates so effectively into the advanced burning phases of massive stars.

3.4. Oxygen Burning Phase

For our stars, core oxygen burning (or O-burning) starts in the temperature range of $(1.5 - 2.6) \times 10^9$ K (see entry 9 in Table 3). One common characteristic of our stars when they evolve to this stage is that they develop convective cores of mass in the range of $(0.77$

- 1.20) M_{\odot} as can be seen in Table 3. These relatively high masses result from the fact that all our sequences have high central mass fractions of ^{16}O after completing core Ne burning. Consequently the effective energy generation rate (nuclear - neutrino) is strongly positive throughout this burning phase and proceeds in a convective core (see Figs. 4 to 10).

We observe from Table 3 (entry 10) that the lifetime of core oxygen burning generally decreases monotonically with stellar mass. Higher mass stars typically burn at higher central temperatures for which the $^{16}\text{O} + ^{16}\text{O}$ reaction is faster. This also explains the difference in lifetimes of core oxygen burning in 25K and 25N. We see from Table 3 that the former model has a longer core oxygen burning lifetime. This is because it evolves at lower central temperature during the early phase of core oxygen burning (see Fig. 13a). Again, we trace back the effect of different rates for $^{12}\text{C}(\alpha, \gamma)^{16}\text{O}$ in these cases.

After core oxygen burning, our models typically show a brief shell neon burning phase followed by a shell oxygen phase. Both of these shells are relatively narrow in extent. Our calculations were not carried beyond shell oxygen-burning.

Finally, we show in Fig. 14 the density and temperature profiles inside our stars as far as we have evolved them, mainly beyond core oxygen burning. The jumps in density seen in Fig. 14a indicate clearly the different cores of the star, where the main fuel of a burning phase is exhausted. Our Fig. 14a is rather similar to Fig. 12 obtained by Limongi et al. (2000).

4. COMPARISON WITH OTHER INVESTIGATIONS

It is worthwhile to compare our results with those obtained by other groups with the aim to find out where a close agreement can be achieved and under which physical conditions. This will help in understanding the complex nature of the advanced burning phases of massive stars and the role of key physical assumptions in the stellar models. Such a comparison, which we present in Tables 5 and 6, is laborious owing to the many parameters involved. Nevertheless, it allows us to consider in detail the three important parameters we have investigated: mass loss, treatment of convection in layers of varying μ -gradient, and the rate of $^{12}\text{C}(\alpha, \gamma)^{16}\text{O}$.

The mass fraction of ^{12}C left over at the end of core helium burning depends on the $^{12}\text{C}(\alpha, \gamma)^{16}\text{O}$ rate and the treatment of the convection. When comparing our results to those obtained by Limongi et al. (2000) (hereafter LSC) in Table 5 & 6, we note that they have evolved their stars at constant mass, used the rate of Caughlan et al. (1985) (hereafter CFHZ85) for $^{12}\text{C}(\alpha, \gamma)^{16}\text{O}$, and treated convection on the basis of the Schwarzschild criterion.

For the $15 M_{\odot}$ star, Table 5 shows that our results are generally in reasonable agreement with theirs where both models apply the same criterion for convection. There is a difference in the central mass fraction of carbon $X(^{12}\text{C})$ in Table 5 & 6) left over at the end of core helium burning: 0.285 in our case compared to 0.195 according to LSC. The reason for our higher values is due to the lower rate of $^{12}\text{C}(\alpha, \gamma)^{16}\text{O}$ we have used (NACRE's compilation, see Fig. 1). The higher value of $X(^{12}\text{C})$ in our case is also responsible for the difference in the lifetime of core C-burning and to the higher mass of the convective core we find. Also the difference in the location and extension of the C-burning shell in our case is also attributable to the higher value of $X(^{12}\text{C})$ which determines the carbon profile in the region of the C-shell. A close agreement is found for the Ne-burning phase. For the core O-burning we find a slightly longer lifetime for our $15 M_{\odot}$ sequence.

Our comparison with the results of WHW in Table 5 & 6 reveals that we can present a similar comparison to what we have done for LSC. We note, however, that WHW have used the rate of $^{12}\text{C}(\alpha, \gamma)^{16}\text{O}$ obtained by Buchmann (1996) but multiplied by a factor of 1.2 in their calculations. In Fig. 1, we see that this is comparable to the rate due to Kunz et al. (2002), which is lower than the NACRE rate we have used in the $15 M_{\odot}$ star for $T_9 < 0.4$. WHW also use a relatively large semiconvective diffusion coefficient implying overshooting, semiconvection, and rotation-induced mixing. Therefore, we think that the relatively low value $X(^{12}\text{C}) = 0.219$ obtained by WHW for the $15 M_{\odot}$ at the end of core He-burning is due to the combined effect of both the $^{12}\text{C}(\alpha, \gamma)^{16}\text{O}$ and the treatment of convection. We may also relate the differences for the location and extent of the C-burning shell compared with WHW to the low value of $X(^{12}\text{C})$ in their model. This also explains the differences during core Ne-burning. Close agreement is found for the core O-burning.

In the case of the $25 M_{\odot}$ sequence, our comparison is presented in Table 6 including four of our sequences (25K, 25N, 25NM, 25L). In this case, mass loss by stellar wind is much higher than in the case of the $15 M_{\odot}$ sequence, as may be seen in the second column of Table 3. Our comparison with the results by LSC will be done with 25NM, which, like the LSC model, was evolved at constant mass. On the other hand, our sequence 25N evolved with the same input physics but included mass loss should reveal the effect of that parameter on the evolution.

We find close agreement between our sequence 25NM and that by LSC during the H-burning and He-burning phases. A slight difference is found for the mass of the helium core and the depth of the convective envelope. The quantities listed in Table 6 for core He-burning are in good agreement with those by LSC, including the $X(^{12}\text{C})$. As expected, the differences are more significant when we compare with our sequence with mass loss (25N). Significantly, the value of $X(^{12}\text{C}) = 0.193$ in 25NM is lower than 0.236 in 25N. The reason for this is that,

toward the end of core He-burning, or, more precisely, when $X(^4\text{He}) \leq 0.10$, the star has evolved to the red giant branch where mass loss increases significantly, as seen in Fig. 15). As a consequence, the star evolves at lower central temperature because it is now a lower mass star. The net result is the high value of $X(^{12}\text{C})$ mentioned above.

Imbriani et al. (2001) have studied the influence of different rates of $^{12}\text{C}(\alpha, \gamma)^{16}\text{O}$ reaction in massive stars. They used the rate of CF88 and that of CFHZ85, which is higher by a factor of $\simeq 2.7$. The CF88 rate led to a central mass fraction of carbon $X(^{12}\text{C}) = 0.424$ at the end of core He-burning, while the second rate led to $X(^{12}\text{C}) = 0.20$. As we have seen, however, when we compare our results for our sequence 25NM with those of LSC, we find close agreement in $X(^{12}\text{C})$ (0.19 in our case to 0.18 in their case). The slight difference is mainly due to the fact that the rate of CFHZ85 for $^{12}\text{C}(\alpha, \gamma)^{16}\text{O}$ used by LSC is about a factor of $1.4 \times$ larger than the NACRE rate we have used in 25NM.

We obtain a longer lifetime for the carbon core phase in 25NM than in LSC's 25 M_\odot model because in 25NM it occurs partly in a convective core of 0.23 M_\odot , which is not present in the case of LSC. During core carbon burning phase, it is known that the neutrino energy losses influences significantly the evolution of the central temperature and density of massive stars. Perhaps the difference in the neutrino loss prescription is partly the cause of the difference in the carbon core evolution. Our neutrino energy losses due to pair, photo, plasma, bremsstrahlung, and recombination processes are taken from the analytical approximation of Itoh et al. (1996). LSC adopted the photo, pair, and plasma neutrino energy losses of Munakata et al. (1985) and Munakata et al. (1986), while their bremsstrahlung neutrino energy loss is taken following Dicus et al. (1976) and Richardson et al. (1982) and their recombination neutrino energy loss follows the prescription of Beaudet et al. (1967). Another contributing factor is the larger value of $X(^{12}\text{C})$ at the end of core helium burning in 25NM than of LSC's 25 M_\odot model which is due to the smaller rate for $^{12}\text{C}(\alpha, \gamma)^{16}\text{O}$ used in 25NM. The presence of a convective core in our case influences strongly the characteristics of the ensuing shell carbon-burning. In the case of 25NM, our first convective carbon-burning shell is located deeper in the star as compared with LSC (see Table 6). The reason is that the presence of a convective core in our case leads to the formation of a steep carbon gradient near to its edge, such that the high carbon abundances drives convection. Note that we have close agreement with LSC concerning the locations of the convective carbon-burning shell in the case of the 15 M_\odot star where a convective core is found in both calculations.

Among our 25 M_\odot models, it is most useful to compare 25K to the 25 M_\odot model of WHW. This is because WHW include mass loss and because we have used the rate for $^{12}\text{C}(\alpha, \gamma)^{16}\text{O}$ for this sequence that is closest to the rate used by WHW (based on Buchmann's compilation as mentioned above) in the temperature range of core helium burning (see Fig.

1).

The remarkable differences are: the lifetime of core H-burning and the mass of the He-core are larger in WHW’s sequence. The first indicates a certain degree of overshooting in the prescription of convection and the second is due to semiconvection being used in the region of the H-burning shell. In §3.1, we have described this issue and found close agreement between the calculations by WHW and our results for the sequence 25L. We recall that in this sequence the inhibiting effect of the μ -gradient on convection was taken into account in the region of H-burning shell.

We emphasize that the convective He-burning shell in our sequence 25L (see Fig. 8) has a similar location to that in the calculations of WHW for their $25 M_{\odot}$ star. Compared to our sequence 25K, this zone is shifted by $0.8 M_{\odot}$ outward. This is a consequence of the larger convective core during helium burning. We note that we still have a higher value of $X(^{12}\text{C})$ at the end of core helium burning than obtained by WHW for similar reasons as explained in the case of the $15 M_{\odot}$ above.

During the core C-burning, our calculations show that a convective core is formed with maximum mass that increases with increasing value of $X(^{12}\text{C})$. There is no convective core formed in the calculations by WHW, and this explains the shorter lifetime of C-burning they have obtained as compared with ours. Whether a convective core is formed or not during core C-burning is crucially dependent on the balance between the nuclear energy generation rate and the neutrino loss rate. It is clear that the former is very sensitive to the value of $X(^{12}\text{C})$ retained at the end of core He-burning. The manner in which core C-burning proceeds will of course determine how carbon-shell burning proceeds later. This explains the different locations and extension of the C-burning shell in our calculations. Indeed, if we go back to the $15 M_{\odot}$ sequence in Table 5 and compare our results for the C-shell burning, we find reasonable agreement with others, because all the calculations presented in Table 5 have a convective core during core C-burning. The fact that the more massive star such as $25 M_{\odot}$ which has higher values of temperature and density, and lower degeneracy than the $15 M_{\odot}$ star make the effect of neutrino energy losses more pronounce. Therefore, the different prescription of the neutrino energy losses makes the carbon core evolution differences of the $25 M_{\odot}$ models more evident.

The existence or absence of a convective core during core C-burning will also influence the properties of the Ne-burning phase. It is interesting that the oxygen-burning phase is more robust, such that a reasonable agreement is achieved among different calculations as seen in Table 5 and 6. This is likely due to the dominance of the nuclear energy production over the neutrino losses during the core O-burning phase.

Summing up this discussion, it is clear that the evolution of massive stars through the advanced burning phases (core C-burning and beyond) is quite sensitive to the earlier evolution. This, in turn, means that the nature of the burning in the models in the advanced phases depends strongly on the the effects of mass loss, on the treatment of convection in inhomogeneous stellar layers, and on the central carbon mass fraction retained at the end of core He-burning.

5. CONCLUSIONS

In this work, we have evolved models of stars of mass $15 - 30 M_{\odot}$ through most of their burning phases. We have analyzed the effects of three important physical ingredients on the structures of the stellar models, viz., mass loss by stellar wind, the recently suggested rates for the $^{12}\text{C}(\alpha, \gamma)^{16}\text{O}$ reaction, and the treatment of convection in inhomogeneous stellar layers on the basis of the Ledoux criterion in contrast to the Schwarzschild criterion. We summarize the main results as follows:

- Mass loss has a strong effect on stellar evolution through advanced phases. The larger the star is initially, the more mass loss will decrease the stellar mass. Then the star, having lower mass, will evolve at lower central temperatures and densities, such that less carbon would be destroyed by $^{12}\text{C}(\alpha, \gamma)^{16}\text{O}$ during core He burning. On the other hand, Figs. 3 and 15 show that mass loss increases strongly when the star reaches the red giant branch (RGB).
- Our discussion of the sequence 25L in §3.1 has emphasized that mass loss depends sensitively on the behavior of the hydrogen-burning shell during core He-burning. When convection is inhibited in the hydrogen shell region by including the chocking effect of the μ -gradient, then the star evolves directly to the RGB, such that it loses more mass. The effect of this convection treatment was also that the helium burning shell and the hydrogen-burning shell migrate outward in mass and burn at relatively lower temperatures.
- Our evolutionary sequences 25K, 25N, and 25NM indicate that the central mass fraction of carbon, $X(^{12}\text{C})$ left after core helium burning determines the physical characteristics of the ensuing core carbon burning and shell carbon burning. The larger $X(^{12}\text{C})$ is, the larger is the mass of the convective core during core carbon burning. The formation of such a core in our calculations leads to a steep gradient of carbon at the edge of the core such that shell carbon-burning occurs first in a convective zone

located deeper in the star compared to other calculation in which no convective core is formed (see Table 6).

- Core Ne-burning is also influenced by the characteristics of the preceding burning phases as described in §3.3.
- Core oxygen burning is found to be less sensitive to the preceding burning phases, because the oxygen central mass fraction at the end of core neon-burning is always high. This leads to the dominance of the nuclear energy production over neutrino energy losses, such that a general agreement is found among different calculations (see Table 5 and 6)

From this work, we see the complex sensitivity of the structure and evolution of massive stars to mass loss, convection, and the $^{12}\text{C}(\alpha, \gamma)^{16}\text{O}$ rate. An exact treatment of these three key ingredients to the models is not yet available; therefore, one must remain aware of their effects on stellar models. This becomes especially important when one considers the resulting nucleosynthesis, as we will do in subsequent work.

We are grateful to Donald Clayton for helpful comments and suggestions. This work has been supported by NSF grant AST-9819877 and by grants from NASA’s Cosmochemistry Program and from the DOE’s Scientific Discovery through Advanced Computing Program. M. F. El Eid is grateful to the American University of Beirut (AUB) for a paid research leave and to Clemson University for support and hospitality.

REFERENCES

Anders, E. & Grevesse, N. 1989, *Geochim. Cosmochim. Acta*, 53, 197

Angulo, C., Arnould, M., Rayet, M., Descouvemont, P., Baye, D., Leclercq-Willain, C., Coc, A., Barhoumi, S., Aguer, P., Rolfs, C., Kunz, R., Hammer, J. W., Mayer, A., Paradellis, T., Kossionides, S., Chronidou, C., Spyrou, K., degl'Innocenti, S., Fiorentini, G., Ricci, B., Zavatarelli, S., Providencia, C., Wolters, H., Soares, J., Grama, C., Rahighi, J., Shotter, A., & Lamehi Rachti, M. 1999, *Nuclear Physics A*, 656, 3

Arnett, D. 1996, Supernovae and nucleosynthesis. an investigation of the history of matter, from the Big Bang to the present (Princeton series in astrophysics, Princeton, NJ: Princeton University Press, —c1996)

Arnett, W. D. 1972, *ApJ*, 176, 699

Audi, G. & Wapstra, A. H. 1995, *Nuclear Physics A*, 595, 409

Beaudet, G., Petrosian, V., & Salpeter, E. E. 1967, *ApJ*, 150, 979

Buchmann, L. 1996, *ApJ*, 468, L127

Caughlan, G. R. & Fowler, W. A. 1988, *Atomic Data and Nuclear Data Tables*, 40, 283

Caughlan, G. R., Fowler, W. A., Harris, M. J., & Zimmerman, B. A. 1985, *Atomic Data and Nuclear Data Tables*, 32, 197

Chieffi, A., Limongi, M., & Straniero, O. 1998, *ApJ*, 502, 737

Chiosi, C. & Maeder, A. 1986, *ARA&A*, 24, 329

de Jager, C., Nieuwenhuijzen, H., & van der Hucht, K. A. 1988, *A&AS*, 72, 259

Dicus, D. A., Kolb, E. W., Schramm, D. N., & Tubbs, D. L. 1976, *ApJ*, 210, 481

El Eid, M. F. 1995, *MNRAS*, 275, 983

Imbriani, G., Limongi, M., Gialanella, L., Terrasi, F., Straniero, O., & Chieffi, A. 2001, *ApJ*, 558, 903

Itoh, N., Hayashi, H., Nishikawa, A., & Kohyama, Y. 1996, *ApJS*, 102, 411

Kippenhahn, R. & Weigert, A. 1990, Stellar Structure and Evolution (Stellar Structure and Evolution, XVI, 468 pp. 192 figs.. Springer-Verlag Berlin Heidelberg New York. Also Astronomy and Astrophysics Library)

Kunz, R., Fey, M., Jaeger, M., Mayer, A., Hammer, J. W., Staudt, G., Harissopoulos, S., & Paradellis, T. 2002, *ApJ*, 567, 643

Langer, N., El Eid, M. F., & Fricke, K. J. 1985, *A&A*, 145, 179

Langer, N., Fricke, K. J., & Sugimoto, D. 1983, *A&A*, 126, 207

Limongi, M., Straniero, O., & Chieffi, A. 2000, *ApJS*, 129, 625

Munakata, H., Kohyama, Y., & Itoh, N. 1985, *ApJ*, 296, 197

—. 1986, *ApJ*, 304, 580

Nomoto, K. & Hashimoto, M. 1988, *Phys. Rep.*, 163, 11

Rauscher, T. & Thielemann, F. 2000, *Atomic Data and Nuclear Data Tables*, 75, 1

Richardson, M. B., van Horn, H. M., Ratcliff, K. F., & Malone, R. C. 1982, *ApJ*, 255, 624

Stothers, R. B. & Chin, C. 1992, *ApJ*, 390, 136

The, L.-S., El Eid, M. F., & Meyer, B. S. 2000, *ApJ*, 533, 998

Woosley, S. E., Heger, A., & Weaver, T. A. 2002, *Reviews of Modern Physics*, 74, 1015

Woosley, S. E., Langer, N., & Weaver, T. A. 1993, *ApJ*, 411, 823

Woosley, S. E. & Weaver, T. A. 1986, *ARA&A*, 24, 205

Table 1. List of Stellar Sequences Studied

Star Mass (M_{\odot})	Massloss	$^{12}\text{C}(\alpha, \gamma)^{16}\text{O}$	$^{22}\text{Ne}(\alpha, \text{n})^{25}\text{Mg}$
15	yes	NACRE ^a	NACRE
20	yes	NACRE	NACRE
25K	yes	Kunz ^b	NACRE
25L ^c	yes	Kunz	NACRE
25N	yes	NACRE	NACRE
25NM	no	NACRE	NACRE
30	yes	NACRE	NACRE

^aRates according to Angulo et al. (1999).

^bRates according to Kunz et al. (2002).

^cThis sequence is obtained by adopting the Ledoux criterion for convection in the regions of the H-burning shell (see Chap. 3.1)

Table 2. Surface Abundance Ratios (by numbers)

	15	20	25N	25NM	25L	30	Initial Value
$^{12}\text{C}/^{13}\text{C}$	18.2	17.8	15.6	28.9	17.49	7.94	90.0
	18.4	16.4	8.63
	93	91	...	90
$^{14}\text{N}/^{15}\text{N}$	2489	3416	7140	3334	2469	20681	271

	2132	2702	...	2977
$^{16}\text{O}/^{17}\text{O}$	930	1054	1022	1366	1309	699	2622
	1231	1433	1159
	881	919	...	1052
$^{16}\text{O}/^{18}\text{O}$	686	705	846	691	614	1976	498
	579	650	1227
	565	574	...	572
[Na/Fe]	0.271	0.361	0.494	0.451	0.302	0.617	0
M_{bottom}/M_{\odot}	3.8	5.8	7.6	7.8	8.7	9.9	
	4.28	6.15	...	8.27	

¹First Row: Present Work, 25N with mass loss, 25M without mass loss.

²Second Row: Schaller et al. (1992).

³Third Row: LSC (2000).

⁴ M_{bottom} is the maximum depth reached by the convective envelope. Values of Schaller et al. are not available.

⁵ $[\text{Na/Fe}] = \log(^{23}\text{Na/Fe})_{star} - \log(^{23}\text{Na/Fe})_{\odot}$

Table 3. CHARACTERISTICS OF EVOLUTIONARY MODELS

stage	Mass (M _⊙)	Evol. Time (yrs)	log(L/L _⊙)	log(T _{eff}) (K)	T _c ^a (10 ⁸ K)	ρ _c ^b (g cm ⁻³)	M _α ^c (M _⊙)	M _{co} ^d (M _⊙)	M _{ONeMg} ^e (M _⊙)	M _{cc} ^{max f} (M _⊙)
<u>15 M_⊙</u>										
1	15.00	0.00	4.277	4.487	0.342	6.28×10 ⁰	0.00	0.00	0.00	5.66
2	14.77	+1.04×10 ⁷	4.617	4.412	0.622	6.33×10 ¹	2.22	0.00	0.00	0.00
3	14.76	+3.40×10 ⁴	4.641	4.237	1.28	1.34×10 ³	2.61	0.00	0.00	2.22
4	13.90	+1.66×10 ⁶	4.690	3.568	3.15	6.53×10 ³	3.85	1.82	0.00	0.00
5	13.84	+2.96×10 ⁴	4.830	3.553	5.67	1.25×10 ⁵	3.85	2.06	0.00	0.55
6	13.82	+6.76×10 ³	4.859	3.550	9.95	4.87×10 ⁶	3.85	2.18	0.44	0.00
7	13.82	+8.63×10 ⁰	4.859	3.550	12.06	8.45×10 ⁶	3.85	2.19	0.88	0.70
8	13.82	+3.13×10 ⁰	4.859	3.550	15.13	6.50×10 ⁶	3.85	2.19	2.01	0.00
9	13.82	+9.82×10 ⁻²	4.859	3.550	15.01	6.73×10 ⁶	3.85	2.19	2.01	0.00
10	13.82	+3.71×10 ⁰	4.857	3.550	19.37	2.13×10 ⁷	3.85	2.19	2.01	0.77
<u>20 M_⊙</u>										
1	20.00	0.00	4.625	4.539	0.359	4.87×10 ⁰	0.00	0.00	0.00	8.72
2	19.45	+7.40×10 ⁶	4.965	4.447	0.729	5.71×10 ¹	3.90	0.00	0.00	0.00
3	19.44	+1.45×10 ⁴	4.991	4.291	1.35	6.59×10 ²	4.21	0.00	0.00	3.70
4	17.34	+1.01×10 ⁶	5.017	3.557	3.46	5.40×10 ³	5.69	3.35	0.00	0.00
5	17.25	+1.42×10 ⁴	5.111	3.547	5.80	4.83×10 ⁴	5.70	3.34	0.00	0.49
6	17.22	+3.30×10 ³	5.135	3.544	10.830	2.77×10 ⁶	5.70	3.52	0.53	0.00
7	17.22	+1.13×10 ¹	5.134	3.544	12.168	6.01×10 ⁶	5.70	3.52	0.80	0.73
8	17.22	+1.21×10 ⁰	5.134	3.544	16.263	4.16×10 ⁶	5.70	3.52	1.16	0.00
9	17.22	+4.88×10 ⁻³	5.134	3.544	16.218	4.23×10 ⁶	5.70	3.52	1.16	0.97
10	17.22	+8.86×10 ⁻¹	5.134	3.544	24.022	1.10×10 ⁷	5.70	3.54	1.77	0.00

Table 3—Continued

stage	Mass (M _⊙)	Evol. Time (yrs)	log(L/L _⊙)	log(T _{eff}) (K)	T _c ^a (10 ⁸ K)	ρ _c ^b (g cm ⁻³)	M _α ^c (M _⊙)	M _{co} ^d (M _⊙)	M _{O_{Ne}Mg} ^e (M _⊙)	M _{cc} ^{max f} (M _⊙)
<u>25 M_⊙ (25C)</u>										
1	25.00	0.00	4.871	4.542	0.325	2.72×10 ⁰	0.00	0.00	0.00	12.6
2	23.94	+6.01×10 ⁶	5.227	4.396	1.06	1.59×10 ²	5.88	0.00	0.00	0.00
3	23.94	+4.60×10 ³	5.238	4.308	1.40	4.20×10 ²	6.00	0.00	0.00	5.35
4	18.49	+7.47×10 ⁵	5.236	3.550	3.62	4.59×10 ³	7.57	4.66	0.00	0.00
5	18.47	+9.70×10 ³	5.309	3.542	6.14	3.71×10 ⁴	7.58	4.86	0.00	0.42
6	18.30	+1.54×10 ³	5.351	3.529	11.58	2.91×10 ⁶	7.58	5.04	0.59	0.00
7	18.30	+5.27×10 ⁻¹	5.319	3.521	12.41	3.64×10 ⁶	7.58	5.04	0.59	0.72
8	18.30	+5.83×10 ⁻¹	5.257	3.526	17.94	3.73×10 ⁶	7.58	5.08	1.53	0.00
9	18.30	+9.58×10 ⁻³	5.253	3.525	18.10	4.17×10 ⁶	7.58	5.08	1.53	1.08
10	18.30	+1.81×10 ⁻¹	5.233	3.529	24.65	1.70×10 ⁷	7.58	5.12	1.80	0.00
<u>25 M_⊙ (25K)</u>										
1	25.00	0.00	4.876	4.575	0.371	4.06×10 ⁰	0.00	0.00	0.00	12.8
2	23.95	+6.00×10 ⁶	5.223	4.397	1.06	1.61×10 ²	5.88	0.00	0.00	0.00
3	23.94	+4.40×10 ³	5.237	4.311	1.39	4.12×10 ²	6.00	0.00	0.00	5.31
4	18.60	+7.49×10 ⁵	5.231	3.550	3.62	4.62×10 ³	7.53	4.67	0.00	0.00
5	18.47	+7.90×10 ³	5.280	3.545	5.51	2.19×10 ⁴	7.54	4.79	0.00	0.47
6	18.41	+3.50×10 ³	5.322	3.540	10.98	2.03×10 ⁶	7.54	5.01	0.45	0.00
7	18.41	+6.93×10 ⁰	5.329	3.541	11.90	4.10×10 ⁶	7.54	5.01	1.09	0.75
8	18.41	+3.28×10 ⁰	5.337	3.538	16.66	4.09×10 ⁶	7.54	5.01	1.09	0.00
9	18.41	+0.00×10 ⁰	5.337	3.538	16.64	4.16×10 ⁶	7.54	5.01	1.09	1.06
10	18.41	+5.10×10 ⁻¹	5.319	3.529	22.75	1.72×10 ⁷	7.54	5.03	2.09	0.00

Table 3—Continued

stage	Mass (M _☉)	Evol. Time (yrs)	log(L/L _☉)	log(T _{eff}) (K)	T _c ^a (10 ⁸ K)	ρ _c ^b (g cm ⁻³)	M _α ^c (M _☉)	M _{co} ^d (M _☉)	M _{O_{Ne}Mg} ^e (M _☉)	M _{cc} ^{max f} (M _☉)
-------	---------------------------	---------------------	------------------------	-------------------------------	--	--	--	---	---	---

<u>25 M_☉ (25N)</u>										
1	25.00	0.00	4.877	4.575	0.371	4.06×10 ⁰	0.00	0.00	0.00	12.8
2	23.94	+5.96×10 ⁶	5.226	4.397	1.053	1.57×10 ²	5.88	0.00	0.00	0.00
3	23.94	+4.30×10 ³	5.237	4.318	1.362	3.86×10 ²	6.00	0.00	0.00	5.32
4	18.67	+7.54×10 ⁵	5.232	3.551	3.624	4.63×10 ³	7.51	4.65	0.00	0.00
5	18.52	+9.60×10 ³	5.304	3.542	6.103	3.61×10 ⁴	7.54	4.85	0.00	0.36
6	18.49	+1.60×10 ³	5.321	3.540	12.11	1.80×10 ⁶	7.54	5.02	0.36	0.00
7	18.49	+1.22×10 ⁻¹	5.320	3.540	12.70	2.11×10 ⁶	7.54	5.02	0.59	0.61
8	18.49	+2.94×10 ⁻¹	5.320	3.540	17.00	2.35×10 ⁶	7.53	5.03	1.46	0.00
9	18.49	+9.14×10 ⁻⁴	5.320	3.540	17.00	2.35×10 ⁶	7.53	5.03	1.46	0.95
10	18.49	+3.31×10 ⁻¹	5.320	3.540	22.59	9.82×10 ⁶	7.53	5.05	1.96	0.00

<u>25 M_☉ (25NM)</u>										
1	25.00	0.00	4.877	4.575	0.371	4.06×10 ⁰	0.00	0.00	0.00	12.8
2	25.00	+5.93×10 ⁶	5.260	4.402	1.06	1.60×10 ²	6.07	0.00	0.00	0.00
3	25.00	+4.30×10 ³	5.272	4.324	1.39	4.07×10 ²	6.20	0.00	0.00	5.20
4	25.00	+7.90×10 ⁵	5.222	3.564	3.65	4.71×10 ³	7.62	4.79	0.00	0.00
5	25.00	+1.01×10 ⁴	5.305	3.555	6.00	3.42×10 ⁴	7.63	4.86	0.00	0.23
6	25.00	+1.86×10 ³	5.322	3.553	11.49	1.83×10 ⁶	7.63	4.92	0.49	0.00
7	25.00	+1.02×10 ⁰	5.322	3.552	12.59	2.71×10 ⁶	7.63	4.92	0.70	0.64
8	25.00	+3.48×10 ⁻¹	5.323	3.552	17.88	3.26×10 ⁶	7.63	4.92	1.59	0.00
9	25.00	+4.12×10 ⁻³	5.323	3.552	17.95	3.38×10 ⁶	7.63	4.92	1.59	1.19
10	25.00	+1.67×10 ⁻¹	5.321	3.552	25.24	5.59×10 ⁶	7.63	4.95	2.35	0.00

Table 3—Continued

stage	Mass (M _⊙)	Evol. Time (yrs)	log(L/L _⊙)	log(T _{eff}) (K)	T _c ^a (10 ⁸ K)	ρ _c ^b (g cm ⁻³)	M _α ^c (M _⊙)	M _{co} ^d (M _⊙)	M _{ONeMg} ^e (M _⊙)	M _{cc} ^{max f} (M _⊙)
<u>25 M_⊙ (25L)</u>										
1	25.00	0.00	4.873	4.572	0.371	4.06×10 ⁰	0.00	0.00	0.00	12.8
2	23.95	+6.02×10 ⁶	5.166	4.453	0.79	5.28×10 ¹	5.61	0.00	0.00	0.00
3	23.95	+9.90×10 ³	5.167	4.222	1.40	4.60×10 ²	5.75	0.00	0.00	6.16
4	13.86	+6.88×10 ⁵	5.336	3.522	3.56	3.94×10 ³	8.34	5.53	0.00	0.00
5	13.66	+7.70×10 ³	5.382	3.522	5.99	2.66×10 ⁴	8.36	5.61	0.00	0.47
6	13.61	+1.88×10 ³	5.382	3.522	11.18	1.94×10 ⁶	8.36	5.69	0.48	0.00
7	13.61	+4.35×10 ⁰	5.382	3.522	12.05	3.63×10 ⁶	8.36	5.72	0.74	0.77
8	13.61	+2.30×10 ⁰	5.382	3.522	17.25	3.65×10 ⁶	8.36	5.72	1.10	0.00
9	13.61	+8.24×10 ⁻³	5.382	3.522	17.27	3.72×10 ⁶	8.36	5.72	1.10	1.15
10	13.61	+4.72×10 ⁻¹	5.382	3.522	22.95	1.82×10 ⁷	8.36	5.75	2.29	0.00
25										
<u>30 M_⊙</u>										
1	30.00	0.00	5.069	4.601	0.381	3.54×10 ⁰	0.00	0.00	0.00	16.10
2	28.25	+5.09×10 ⁶	5.409	4.355	1.25	1.98×10 ²	7.90	0.00	0.00	0.00
3	28.25	+1.80×10 ³	5.415	4.303	1.44	3.13×10 ²	7.98	0.00	0.00	7.17
4	17.07	+6.29×10 ⁵	5.408	3.542	3.74	4.07×10 ³	9.49	6.38	0.00	0.00
5	16.84	+7.00×10 ³	5.463	3.537	6.27	2.84×10 ⁴	9.54	6.50	0.00	0.39
6	15.24	+1.01×10 ³	5.463	3.537	11.92	1.76×10 ⁶	9.54	6.72	0.67	0.00
7	15.24	+7.13×10 ⁻¹	5.463	3.537	12.44	2.37×10 ⁶	9.54	6.75	0.80	0.67
8	15.24	+3.34×10 ⁻¹	5.463	3.537	18.70	3.06×10 ⁶	9.54	6.75	1.69	0.00
9	15.24	+4.58×10 ⁻³	5.463	3.537	18.21	2.68×10 ⁶	9.54	6.75	1.78	1.20
10	15.24	+1.02×10 ⁻¹	5.463	3.537	26.02	4.68×10 ⁶	9.54	6.89	2.80	0.00

Table 3—Continued

stage	Mass (M _⊕)	Evol. Time (yrs)	log(L/L _⊕)	log(T _{eff}) (K)	T _c ^a (10 ⁸ K)	ρ _c ^b (g cm ⁻³)	M _α ^c (M _⊕)	M _{co} ^d (M _⊕)	M _{O_{Ne}Mg} ^e (M _⊕)	M _{cc} ^{max f} (M _⊕)
...										
...										
...										

^aT_C is the central temperature.

^bρ_C is the central density.

^cM_α is the mass size of helium core.

^dM_{co} is the mass size of C/O core.

^eM_{O_{Ne}Mg} is the mass size of O/Ne/Mg core.

^fM_{cc}^{max} is the maximum convective core mass of that burning phase.

*Stages 1 to 10 correspond to the evolutionary time of 1) Zero Age Main sequence, 2) central hydrogen exhaustion, 3) central helium ignition, 4) central helium exhaustion, 5) central carbon ignition, 6) central carbon exhaustion, and 7) central neon ignition, 8) central neon exhaustion, 9) central oxygen ignition, 10) central oxygen exhaustion, respectively.

Table 4. Central ^{12}C and ^{20}Ne Mass Fractions at Central Core Helium and at Central Core Neon Exhaustions, ^{16}O Mass Fractions at Central Core Helium, at Central Core Carbon, and at Central Core Neon Exhaustions

Mass (M_\odot)	$X(^{12}\text{C})$		$X(^{20}\text{Ne})$		$X(^{16}\text{O})$		
	End Helium	End Helium	End Carbon	End Helium	End Carbon	End Carbon	End Neon
15	0.285	0.0028	0.371	0.688	0.548	0.738	
20	0.258	0.0041	0.349	0.713	0.579	0.758	
25K	0.280	0.0052	0.384	0.689	0.541	0.737	
25L	0.274	0.0054	0.379	0.695	0.549	0.740	
25N	0.236	0.0052	0.329	0.733	0.606	0.795	
25NM	0.193	0.0067	0.275	0.774	0.669	0.806	
30	0.221	0.0070	0.316	0.745	0.624	0.786	

Table 5. Comparison of $15 M_{\odot}$ Models

Physical Quantity	PW ^a	LSC ^b	WHW ^c
H-Burning			
$\tau_H (10^6 \text{ yr})$	10.4	10.7	11.1
$M_{cc} (M_{\odot})$	5.66	6.11	5.7
$M_{C\text{-envelope}}^{final}$	3.94	4.28	4.5
M_{core}^*	3.85	4.10	4.15
He-Burning			
$\tau_{He} (10^6 \text{ yr})$	1.66	1.40	1.97
$M_{cc} (M_{\odot})$	2.22	2.33	2.60
$M_{core} (M_{\odot})$	2.27	2.39	2.80
$X(^{12}\text{C})/X(^{16}\text{O})$	0.285/0.688	0.195/0.777	0.216/-
ΔM (He-shell) (M_{\odot})	2.3-3.1	2.43-3.54	2.8-4.2
C-Burning			
$\tau_C (10^3 \text{ yr})$	6.76	2.60	2.03
$M_{cc} (M_{\odot})$	0.55	0.41	0.50
$M_{core} (M_{\odot})$	2.01	2.44	1.85
ΔM (C-shell) (M_{\odot})	0.50-1.21 0.99-1.76 1.38-1.91 1.56-1.67 1.64-2.18	0.39-0.80 0.80-1.18 1.20-1.77 1.90-2.61	0.59-1.20 1.20-2.30 1.90-2.61
Ne-Burning			
τ_{Ne} (yr)	1.98	2.00	0.73
$M_{cc} (M_{\odot})$	0.70	0.66	0.70
$X(^{16}\text{O})/X(^{24}\text{Mg})$	0.74/0.09	0.81/0.05	-
O-Burning			
τ_O (yr)	3.71	2.47	2.58
$M_{cc} (M_{\odot})$	0.77	0.94	0.80

^a M_{core} means in this and the following Table the region in which the fuel of the burning phase has been exhausted.

Table 6. Comparison of $25 M_{\odot}$ Models

Physical Quantity	25K	25N	25NM	LSC	25L	WHW
H-Burning						
$\tau_H (10^6 \text{ yr})$	6.00	6.00	5.93	5.93	6.02	6.70
$M_{cc} (M_{\odot})$	12.8	12.8	12.8	12.8	12.8	12.5
M_{core}	7.54	7.53	7.63	8.01	8.36	8.43
$M_{conv.-env.}^{final}$	7.60	7.60	7.89	8.27	8.71	8.60
He-Burning						
$\tau_{He} (10^6 \text{ yr})$	0.749	0.754	0.79	0.68	0.688	0.839
$M_{cc} (M_{\odot})$	5.31	5.32	5.20	5.23	6.16	6.50
$M_{C/O-core} (M_{\odot})$	5.03	5.05	4.95	4.90	6.09	6.45
$X(^{12}\text{C})/X(^{16}\text{O})$	0.28/0.69	0.24/0.73	0.19/0.77	0.18/0.79	0.27/0.70	0.19/-
ΔM (He-shell) (M_{\odot})	5.30-6.30	5.30-6.30	5.25-7.35	5.30-7.68 ^a	6.28-8.07	6.5-8.1
C-Burning						
τ_C (yr)	3500	1600	1860	970	1880	522
$M_{cc} (M_{\odot})$	0.47	0.36	0.23	radiative	0.47	radiative
$M_{core}^* (M_{\odot})$	2.50	1.96	2.63	2.40	2.61	2.45
ΔM (C-shell) (M_{\odot})	0.50-1.19 1.30-4.54	0.38-0.97 1.04-2.19	0.865-1.16 1.21 - 3.12	1.48-2.43 2.28-4.61	0.52-1.30 1.33-5.15	1.60-5.60 3.20-5.70
		2.26-4.94	2.76 - 3.50			
Ne-Burning						
τ_{Ne} (yr)	3.28	0.294	0.348	0.77	4.35	0.89
$M_{cc} (M_{\odot})$	0.75	0.61	0.64	0.50	0.77	1.0
$M_{core} (M_{\odot})$	1.80	1.96	2.16	2.29	2.05	2.20
$X(^{16}\text{O})/X(^{24}\text{Mg})$	0.74/0.10	0.80/0.09	0.81/0.07	0.83/0.05	0.74/0.10	-
O-Burning						
τ_O (yr)	0.510	0.33	0.547	0.33	0.47	0.40
$M_{cc} (M_{\odot})$	1.06	0.95	1.19	1.15	1.15	1.25

*The definition of M_{core} is somewhat ambiguous, one should see the carbon profile for more detail.

^aWe took the second broad convective He-shell obtained by Limongi et al. (2000) which resembles ours.

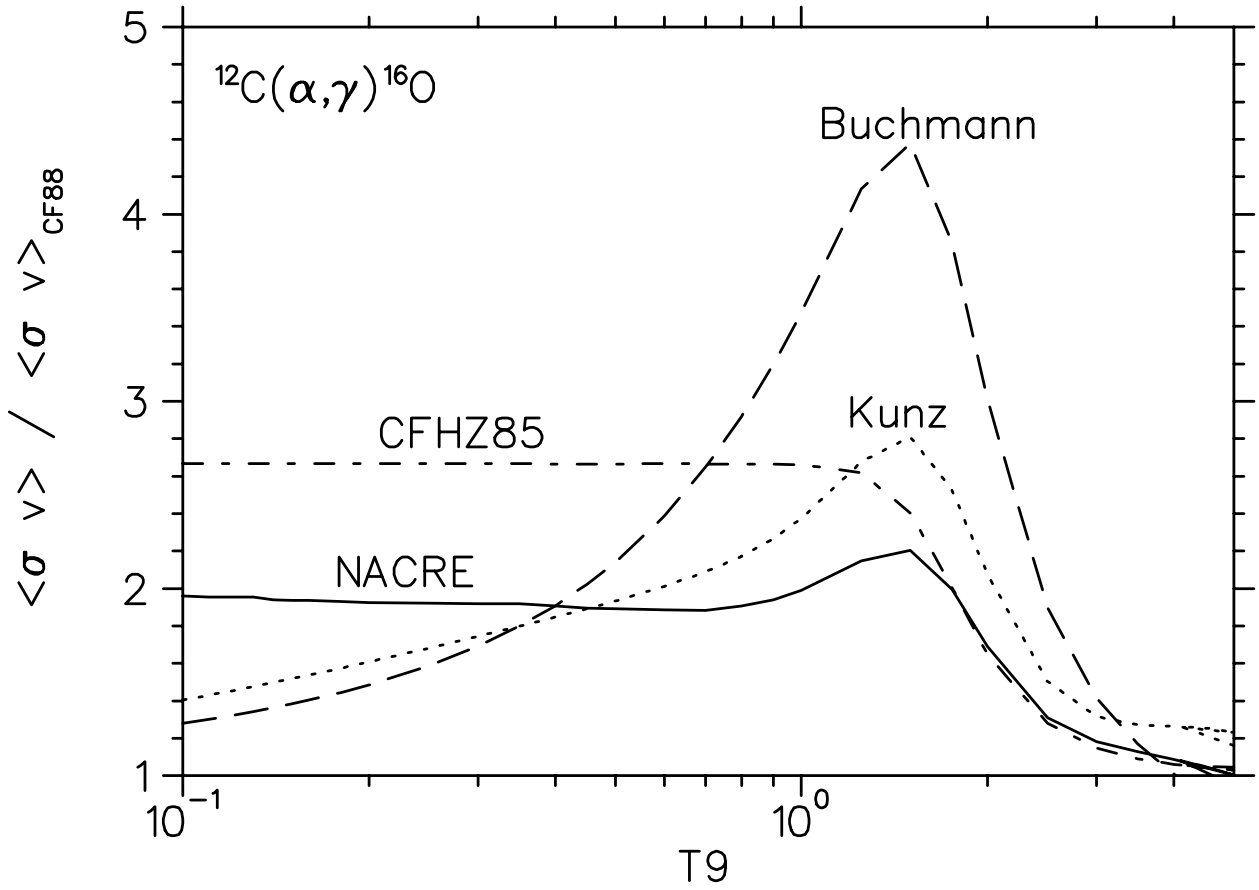


Fig. 1.— Comparison of the $^{12}\text{C}(\alpha, \gamma)^{16}\text{O}$ reaction rates among different compilations. See text for references. Note that core helium burning occurs in the range $T_9 = 0.13 - 0.40$ for the stars under investigations in this paper (see Table 3).

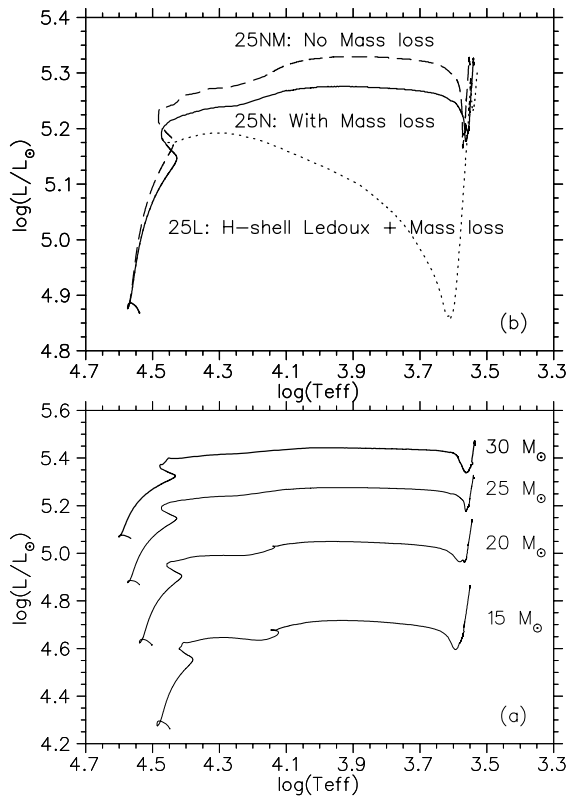


Fig. 2.— Hertzsprung-Russell diagram for the stars studied in this work (a). See Table 1 for more information about these tracks. The Hertzsprung-Russell diagram for the $25 M_\odot$ star evolved with different assumptions (b). A significant difference between these tracks is clearly seen.

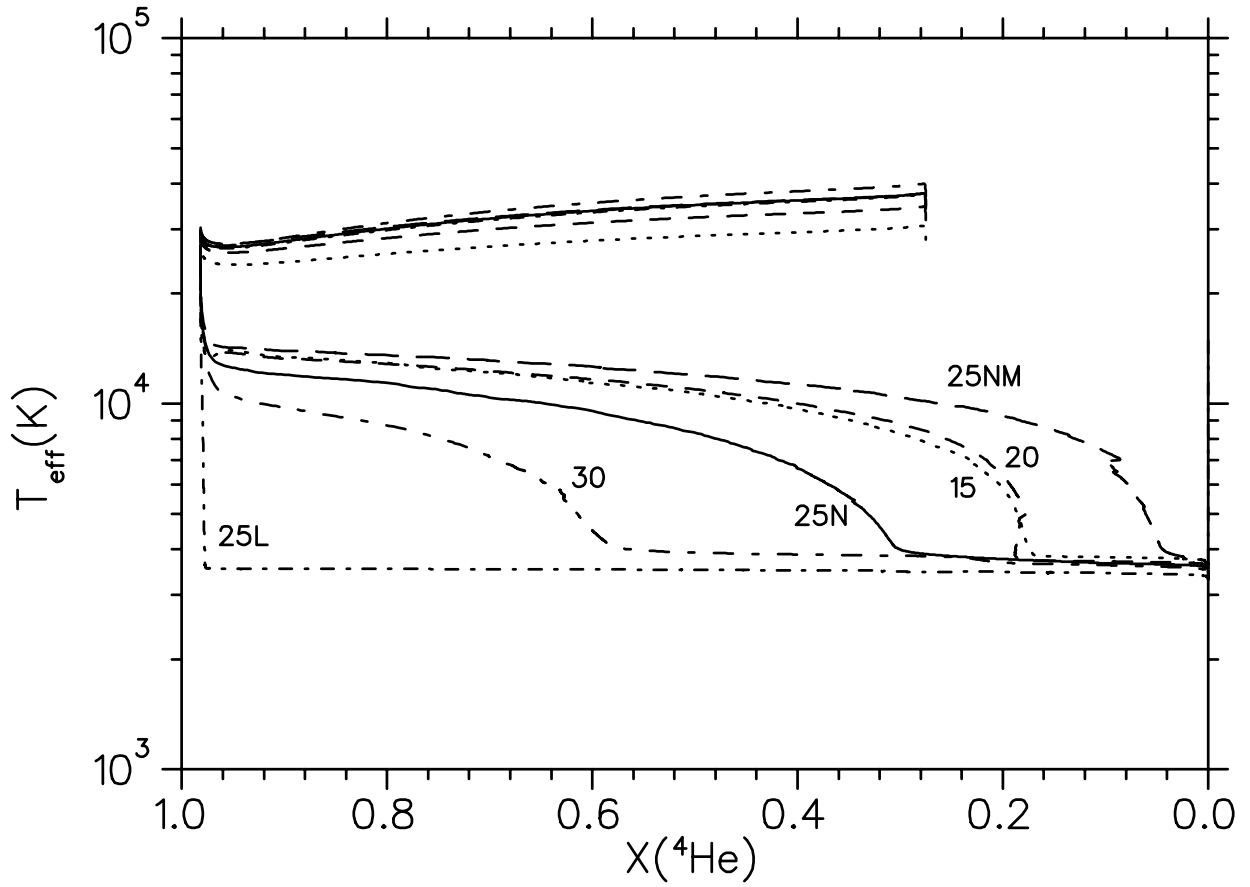


Fig. 3.— Evolution of the stars under consideration in a T_{eff} - $X(^4\text{He})$ plane, where $X(^4\text{He})$ is the central mass fraction of helium. Note the different timing of the transition to the red giant branch during core He-burning in particular the immediate evolution of 25L to that stage.

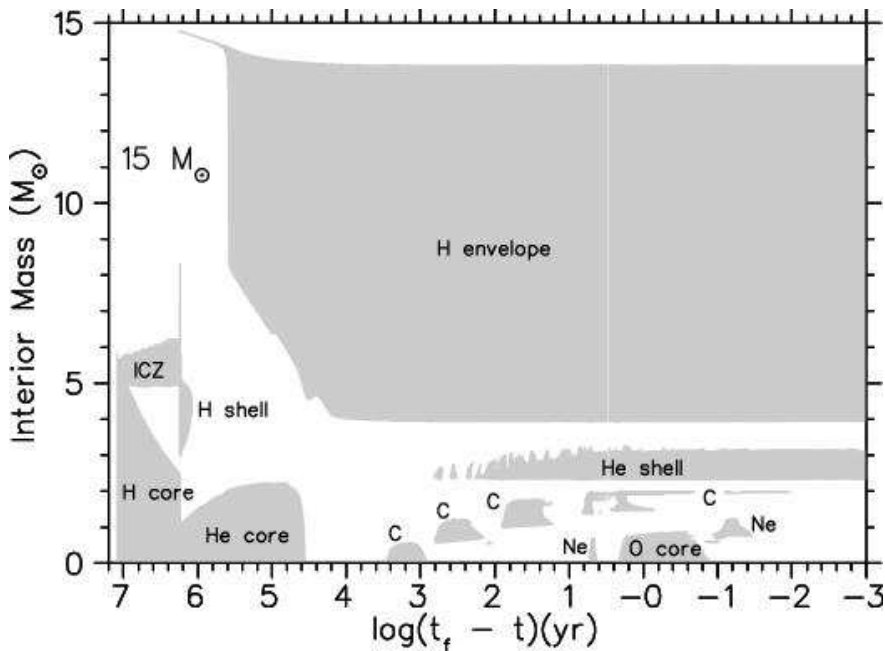


Fig. 4.— The change of the internal structure as a function of time of the $15 M_{\odot}$ star of initial solar-like composition. The star is evolved with mass loss by stellar wind from the main sequence till oxygen shell-burning. Each vertical line corresponds to a stellar model at a given time. Convective regions are labeled according to their physical origin, see text for details. Note that the t_f is the time of the last stellar calculated and the t is the evolution time. For example core hydrogen burning in this diagram starts at $\log(t_f - t) = 7.02$, or $10^{7.02}$ years from the time of the last model.

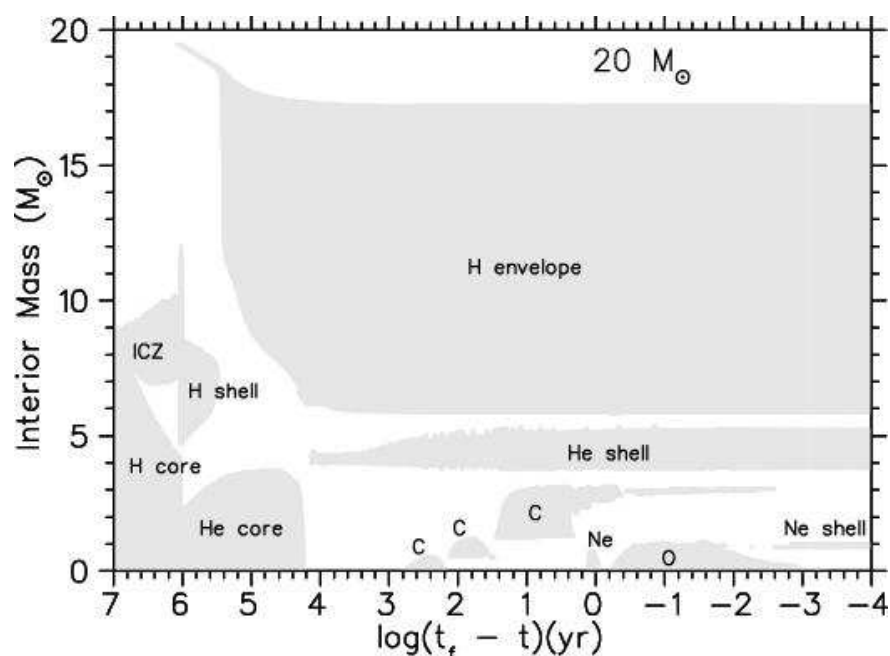


Fig. 5.— Same as Fig. 4 for the $20 M_{\odot}$ star.

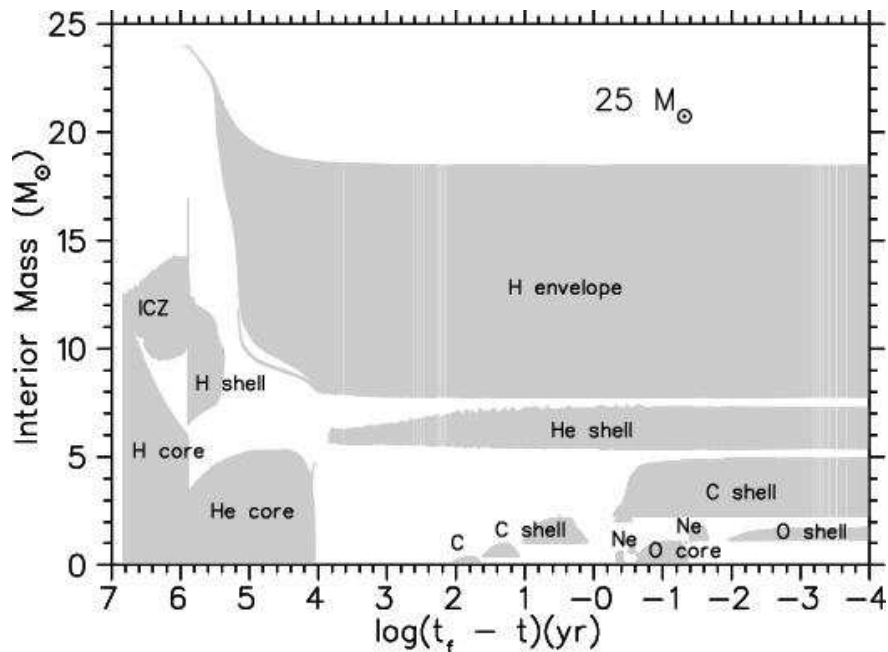


Fig. 6.— Same as Fig. 4 for a $25 M_{\odot}$ star (sequence 25N), (see Table 1 for more information). Note that the convective zone above the H-burning shell dies out before the end of core He-burning in contrast to Fig. 9 without mass loss.

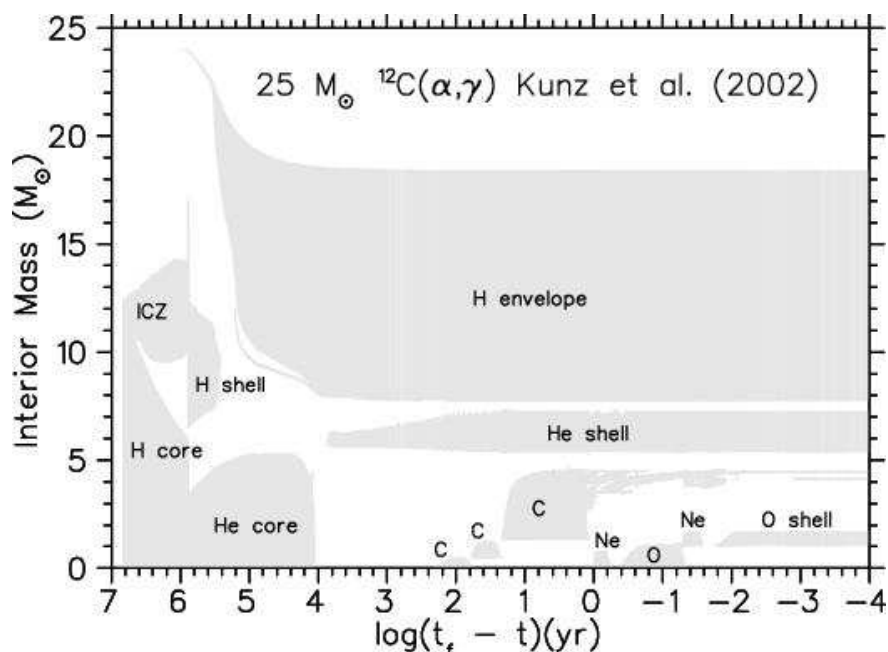


Fig. 7.— Same as Fig. 4 for the sequence 25K (See Table 1 for more information).

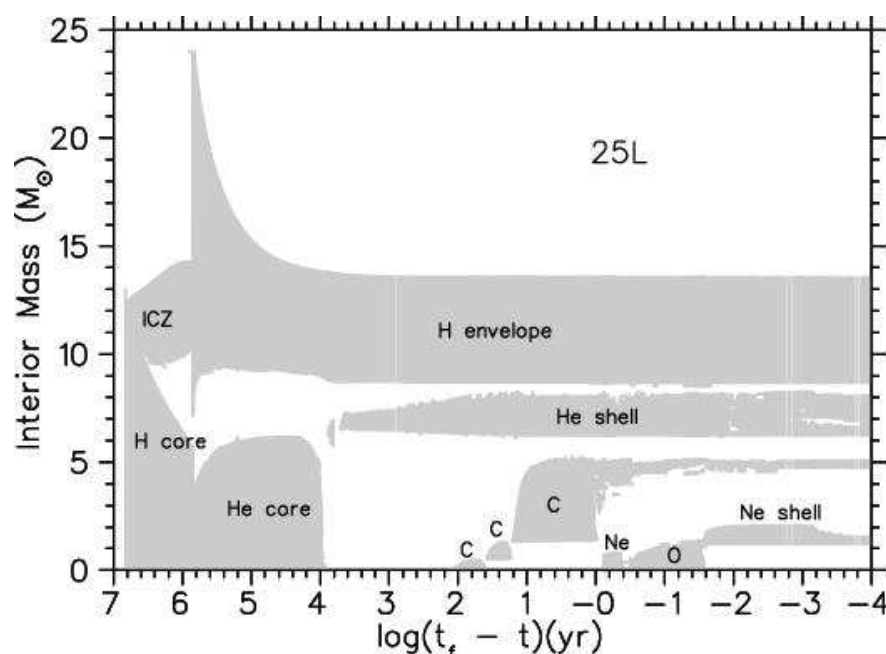


Fig. 8.— Same as Fig. 4 for the sequence 25L (See Table 1 for more information).

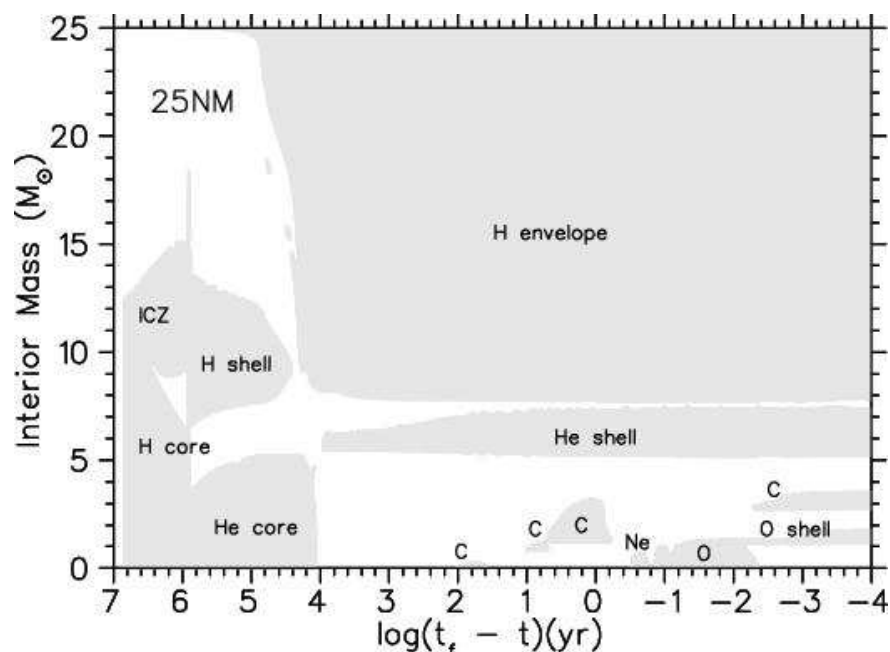


Fig. 9.— Same as Fig. 4 for the sequence 25NM (See Table 1 for more information).

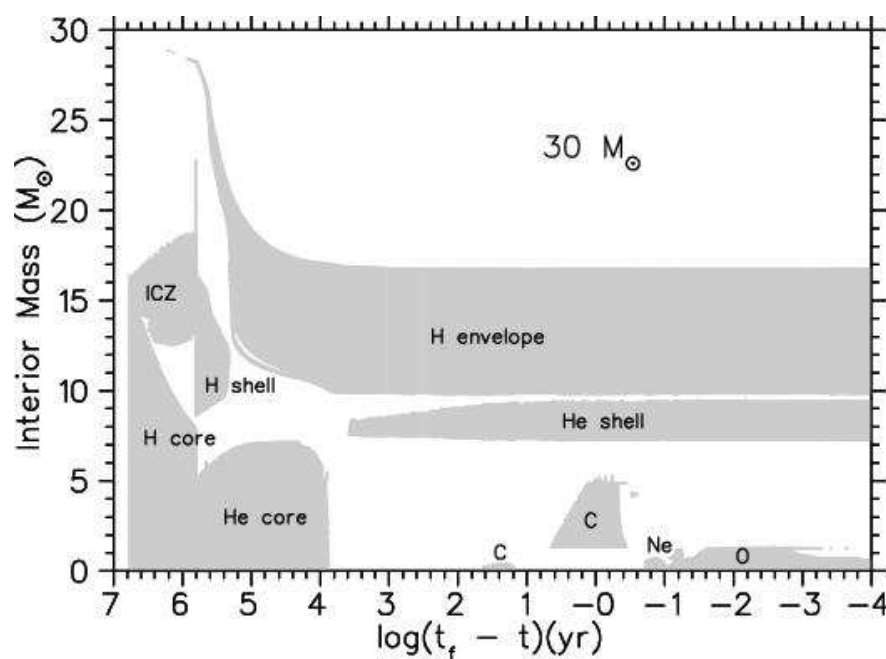


Fig. 10.— Same as Fig. 4 for the star of $30 M_{\odot}$.

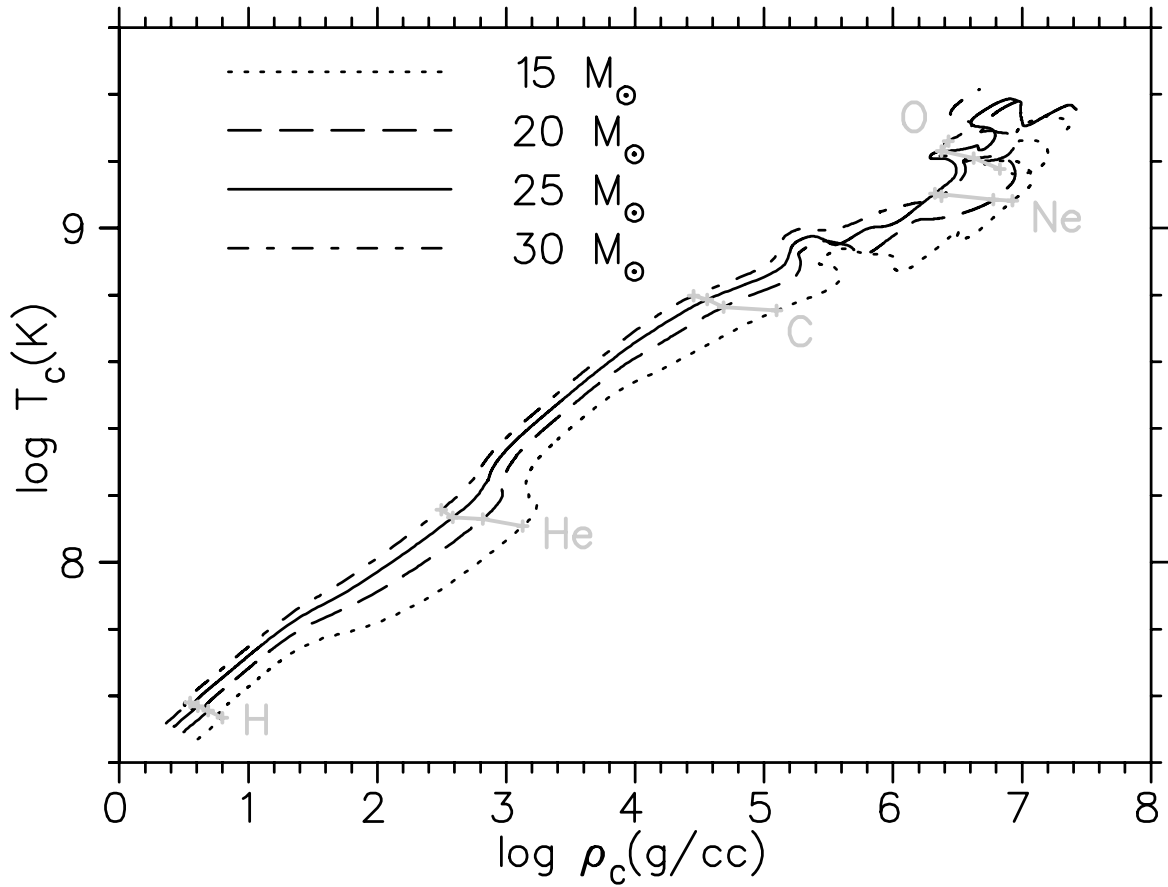


Fig. 11.— Central Temperature T_C versus central density ρ_C for the stars of masses $15 M_\odot$ to $30 M_\odot$. The lines marking H, He, C, Ne, and O indicate at which T_C and ρ_C a burning phase starts.

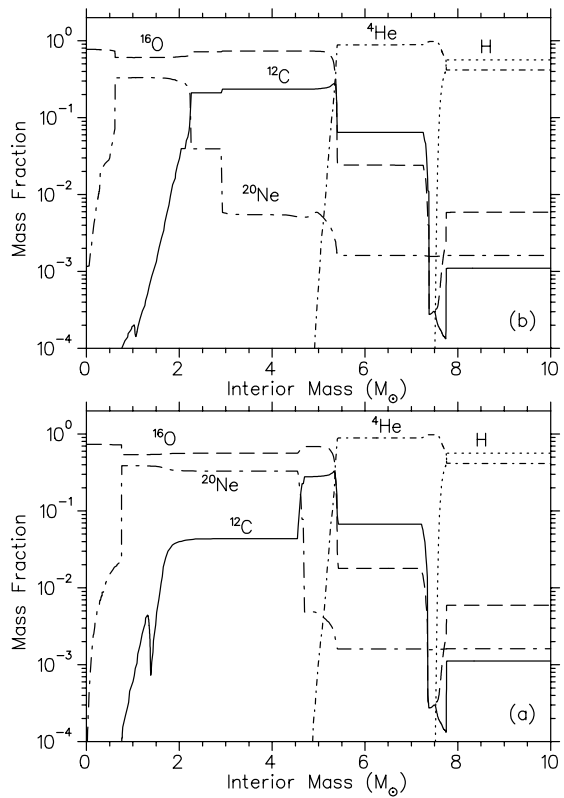


Fig. 12.— Composition profile for the sequence 25K (a) and the sequence 25N (b) versus interior mass at the end of core Ne-burning.

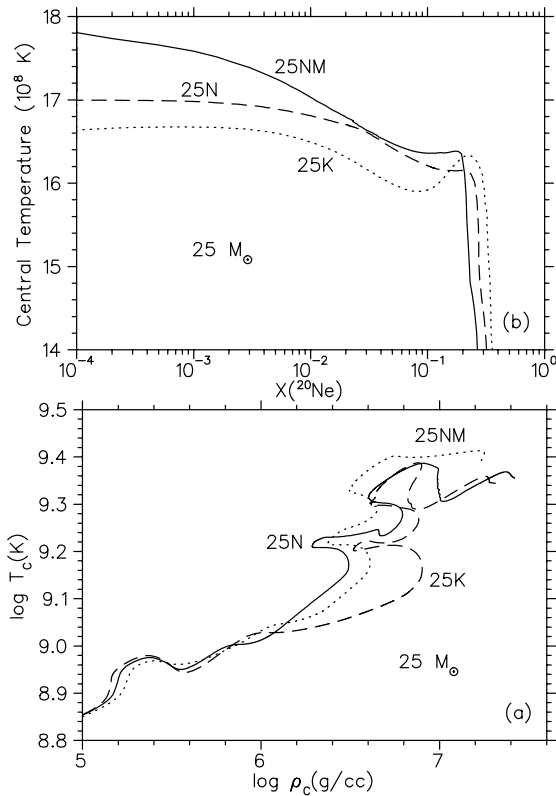


Fig. 13.— (a) Similar to Fig. 11 showing only the evolution of the center of the $25 M_\odot$ star under different assumptions (See Table 1). (b) Central Temperature T_C versus the central mass fraction of ²⁰Ne, $X(^{20}\text{Ne})$. The curves illustrate how T_C evolves differently through the core Ne-burning phase under different assumptions (see 3.3 for details).

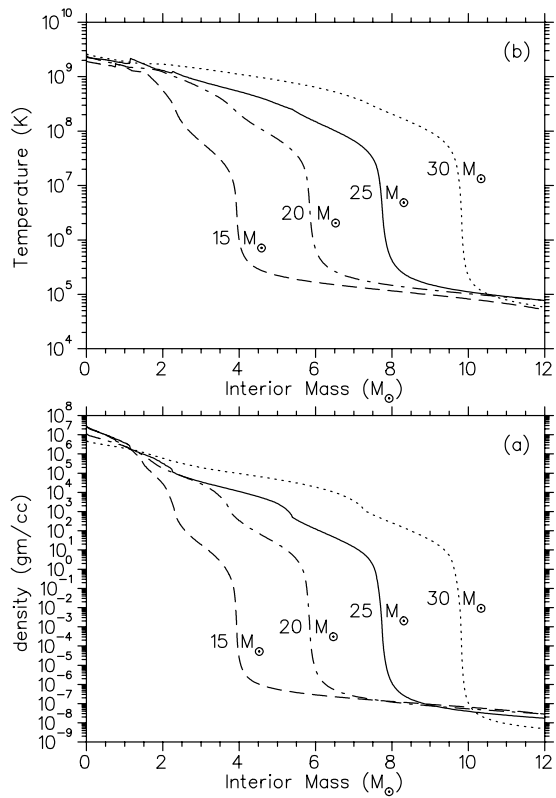


Fig. 14.— Density (a) and temperature (b) versus interior mass for the stars of masses 15 M_\odot to 30 M_\odot as they evolved past core oxygen burning.

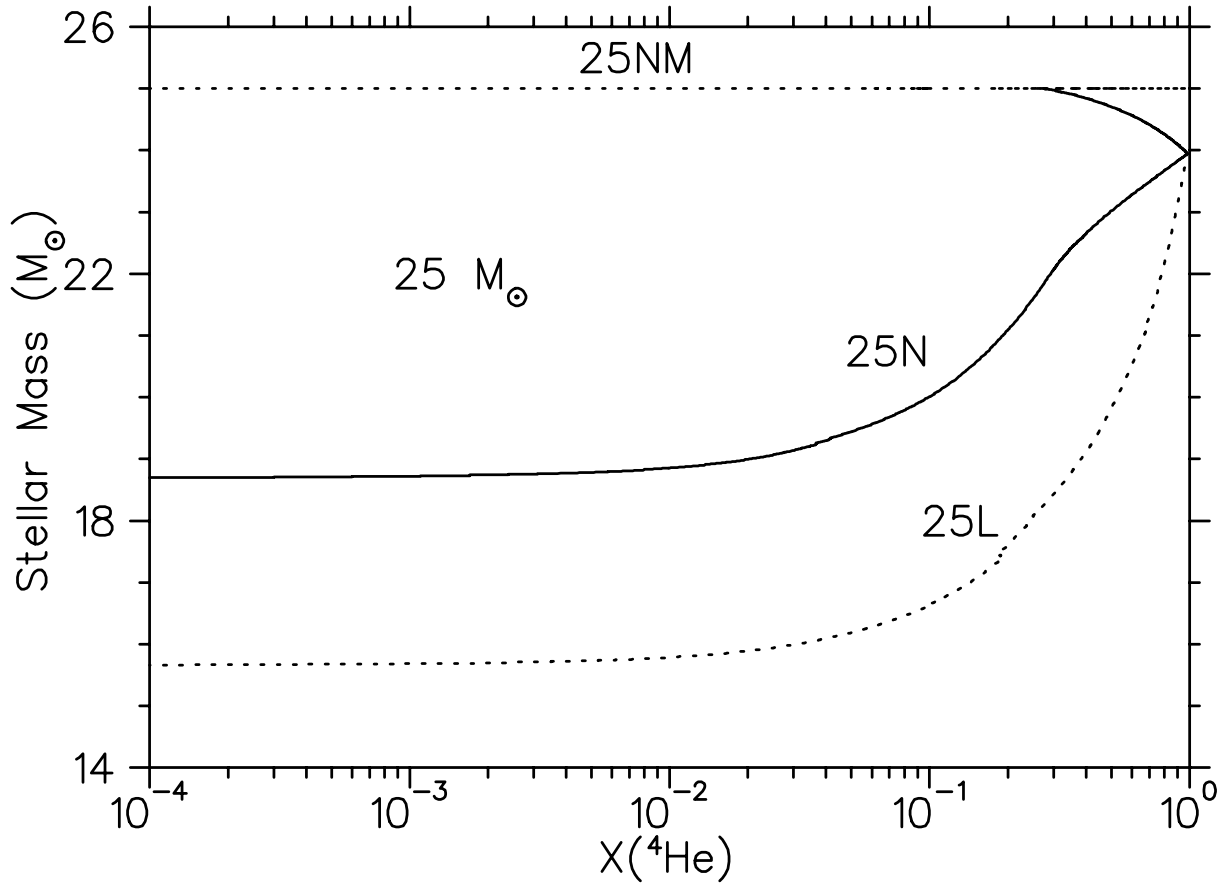


Fig. 15.— Stellar mass versus central mass fraction of Helium, $X(^4\text{He})$ for the $25 M_\odot$ star with and without mass loss. Notice the sharp decrease of the stellar mass during the late phase of core He-burning ($X(^4\text{He}) \leq 0.1$).